Applied Surface Science 501 (2020) 144217

Contents lists available at ScienceDirect

Applied Surface Science

journal homepage: www.elsevier.com/locate/apsusc

Full Length Article

Synthesis of γ-Fe_2O_3-ZnO-biochar nanocomposites for Rhodamine B removal

Ying Zhang[a,1], Peidong Su[a,1], Daria Weathersby[a], Qinku Zhang[a], Jinju Zheng[c], Ruimei Fan[d], Junke Zhang[b], Qilin Dai[a,*]

[a] Department of Chemistry, Physics and Atmospheric Sciences, Jackson State University, Jackson, MS 39217, USA
[b] Department of Civil and Environmental Engineering, Jackson State University, Jackson, MS 39217, USA
[c] Institute of Materials, Ningbo University of Technology, Ningbo City 315016, China
[d] Civil and Environmental Engineering Department, The University of Delaware, Newark, DE 19716, USA

ARTICLE INFO

Keywords:
Biochar
Rhodamine B
Magnetic
Nanocomposite
Photocatalyst

ABSTRACT

Organic dye molecules, for example Rhodamine B (RhB), cause a serious environmental issue in industry wastewater. Magnetic biochar adsorption is one of the effective ways for water treatment. In this work, we develop a facile technique to synthesize magnetic biochar γ-Fe_2O_3-ZnO-biochar nanocomposites by thermal decomposition of zinc(II) acetylacetonate and iron(III) 2,4-pentanedionate in the presence of biochar in triethylene glycol solvent under the protection of nitrogen. The synthesized magnetic biochar nanocomposites are characterized using X-ray diffraction (XRD), transmission electron microscopy (TEM), scanning electron microscope (SEM), and their adsorption performance on RhB is investigated. The adsorption capabilities of the nanocomposites are controlled by the ratios of zinc(II) acetylacetonate: iron(III) 2,4-pentanedionate: biochar, which provides an easy way to optimize the adsorption performance of the nanocomposites. The removal RhB tests indicate that magnetic γ-Fe_2O_3-ZnO-biochar nanocomposites exhibit improved performance than bare biochar. The improved performance is attributed to photocatalyst properties of ZnO in the composite. The developed method represents a novel strategy to prepare magnetic biochar nanocomposites with improved removal capabilities via photocatalyst nanoparticles toward wastewater treatment.

1. Introduction

Rhodamine B (RhB) is a typical kind of industrial dye molecules which is widely used in paper printing, textile and leather industries. However, RhB is a very common contaminant in waste water. Therefore, removal of RhB from waste water is very necessary not only for fundamental studies but also for aquatic life and human health. The common methods for removal of RhB include coagulation/flocculation [1], photocatalytic degradation [2], electrochemical oxidation [3] and adsorption [4]. Adsorption is considered to be economical, cost-effective and efficient for dye removal [5,6]. Biochar has received much attention as an adsorbent to remove dye molecules from waste water due to its excellent adsorption performance caused by the large area [7]. Moreover, magnetic biochar with the advantage of separating adsorbents from aqueous solutions are extensively studied in the waste water treatment [8,9]. However, the biochar adsorption capability is reduced due to the decreased surface area caused by the magnetic components in the composites, which limits the application of magnetic biochar [10,11]. Usually, metal salts, for example $FeCl_3$, are used as starting materials for magnetic biochar preparation, which requires high temperature annealing process, for example coprecipitation method, and it is difficult to control the distribution of magnetic nanoparticles in the biochar matrix. In addition, the traditional synthesis routes of magnetic biochar are complex and time-consuming [12]. Therefore, the investigation of magnetic biochar synthesis methods toward facile preparation techniques and excellent adoption capability is very necessary to the development of magnetic biochar in the application of waste water treatment. Another effective method for organic dye removal is photocatalytic degradation. Semiconductor, such as ZnO and TiO_2, are commonly used photocatalysts for organic dye removal [13–17]. The electron hole pairs generated from photoexcitation and promotion lead to the generation of reactive oxygen species (ROS), and then the e- - h+ and ROS could react with organic dye resulting degradation [18]. In addition, it is reported that ZnO with controllable surface energy shows potential application in photoelectrocatalytic degradation of organic dyes [18–24]. Taking advantage photocatalytic degradation of ZnO nanoparticle could improve the removal efficiency of magnetic biochar.

* Corresponding author.
E-mail address: qilin.dai@jsums.edu (Q. Dai).
[1] These two authors contribute equally to this work.

https://doi.org/10.1016/j.apsusc.2019.144217
Received 15 May 2019; Received in revised form 20 August 2019; Accepted 28 September 2019
Available online 05 October 2019
0169-4332/

This study presents a novel one-step synthesis method of magnetic γ-Fe_2O_3-ZnO-biochar nanocomposites using thermal decomposition of zinc(II) acetylacetonate and iron(III) 2,4-pentanedionate in the presence of biochar in triethylene glycol under the protection of nitrogen. This method avoids the high temperature annealing process, and the adsorption capability of the magnetic biochar is also improved by ZnO due to the photocatalysis properties. The structure and properties of the synthesized nanocomposites with different ratios of iron(III) 2,4-pentanedionate:zinc(II) acetylacetonate:biochar are studied. The adsorption properties of RhB by magnetic biochar nanocomposites are studied by decoloration of RhB under UV-light. The influence of the ratios of iron(III) 2,4-pentanedionate: zinc(II) acetylacetonate: biochar on RhB removal is investigated to demonstrate the improved RhB removal capability by our magnetic biochar.

2. Materials and methods

2.1. Materials

The powder biochar was purchased from BiocharNow Inc. Rhodamine B (Pure), Triethylene glycol (99%) and zinc(II) acetylacetonate (25% Zn) were purchased from Acros organics. Iron(III) 2,4-pentanedionate was obtained from Alfa Aesar. Ethanol anhydrous (histological grade) was purchased by Fisher Chemical Co., Ltd. All the chemicals were utilized directly without any further purification.

2.2. Synthesis of γ-Fe_2O_3-ZnO-biochar nanocomposites

The γ-Fe_2O_3-ZnO-biochar nanocomposites were synthesized using thermal decomposition of zinc(II) acetylacetonate and iron(III) 2,4-pentanedionate in the presence of biochar in triethylene glycol under the protection of nitrogen. In this typical synthesis process, biochar and triethylene glycol were placed into a 100 mL three-neck flask. The flask was sealed and sonicated for 10 min to ensure mixing. After that, iron (III) 2,4-pentanedionate and zinc(II) acetylacetonate were immediately added into the mixture under vigorous stirring. The mixture was heated to 120 °C followed by degassing and purging with N_2 gas for three times. The resulting mixture was then heated to 180 °C for 30 min followed by heating up to 275 °C for designed reaction time. Then the harvested biochar nanocomposites were washed by ethanol anhydrous for 5 times, and then the final products were obtained by drying in a vacuum. The detailed information of the synthesis parameters and the sample information are summarized in Table 1.

2.3. Characterization

The morphology of samples was investigated by scanning electron microscopy (SEM) and Transmission electron microscope (TEM). SEM images were obtained by TESCAN LYRA3. TEM images were collected using a JEM-1011 Transmission Electron Microscope (JEOL). The XRD diffraction patterns were carried out using MiniFlex600 (Rigaku) using a Cu-Kα radiation at 40 kV/15 mA. The 2-theta ranged from 10° to 80° was used for XRD measurement. XPS analysis was performed using a Thermo-Fisher ESCALAB Xi+ spectrometer equipped with a monochromatic Al X-ray source (1486.6 eV, 300 mm2 spot size). Measurements were performed using the standard magnetic lens mode and charge compensation. The base pressure in the analysis chamber during spectral acquisition was 3×10^{-7} mBar. Spectra were collected at a take off angle of 90° from the plane of the surface. The pass energy of the analyzer was set at 20 eV for high-resolution spectra and 150 eV for survey scans, with energy resolutions of 0.1 eV and 1.0 eV, respectively. Binding energies were calibrated with respect to C 1 s at 284.8 eV. All spectra were recorded using the Thermo Scientific Avantage software; data files were translated to VGD format and processed using the Thermo Avantage package v5.9904. Brunauer–Emmett–Teller (BET) surface area and pore structure of sample were tested by TriStar II Plus.

Table 1
Synthesis parameters of iron(III) 2,4-pentanedionate:zinc(II) acetylacetonate: biochar ratio nanocomposites and sample information.

Sample	Ratio (g:g:g)	Reaction time at 275 °C (h)
S1	4:0:2	0.5
S2	4:1:2	0.5
S3	4:1:2	1.5
S4	4:1:2	3.0
S5	2:1:2	0.5
S6	8:1:2	0.5
S7	4:2:2	0.5
S8	4:4:2	0.5
S9	0:2:2	0.5
S10	0:4:2	0.5
S11	0:8:2	0.5

2.4. Adsorption and photocatalytic decoloration test

For the adsorption tests, 20 mL of RhB aqueous solution (0.01 mol/L) was added into a 50 mL beaker by mixing with certain amount of biochar nanocomposites directly. For a single adsorption, 0.03 g biochar, 0.0432 g S1, 0.0478 g S2, 0.0478 g S3, 0.0478 g S4, 0.0412 g S5, 0.061 g S6, 0.0524 g S7, 0.062 g S8, 0.039 g S9, 0.0485 g S10, 0.067 g S11 was used. In this way, the same amount of biochar for all the samples was involved in all tests. The suspension was homogenized and placed in the dark environment with continuous stirring at 200 rpm for 15 min. The suspension was then filtered immediately through a 0.45 μm syringe filter, the residual content of RhB was measured using a UV–vis spectrophotometer (Cary60, Aligent Technologies). The adsorption percentage of RhB of the biochar nanocomposite was then determined according to the following equation:

$$\eta = \frac{(C_0 - C_e)}{C_0} \times 100\% \quad (1)$$

where η (%) represents the adsorption percentage of RhB. C_0 and C_e (mg/L) are the initial concentration and equilibrium concentration of RhB solution, respectively.

The photocatalytic performances of synthesized biochar nanocomposites were examined by investigating the decoloration of RhB solutions. The raw homogenized solutions after adsorption by biochar nanocomposites for 15 min were illuminated under UV-light for another period of 30 min. The distance between the light source and top of solution was about 10 cm. The UV lamp is BLAK-RAY Ultraviolet Lamp (Model B 100 AP). The real power inside the beaker was 16.45 MED/hr (tested by Model PMA2100 Dual Input Radiometer). The obtained solutions were then filtered by 0.45 μm syringe filter and the concentrations of RhB in the solution were measured by UV–Vis spectrophotometer.

3. Results and discussion

3.1. Characterization of the synthesized biochar nanocomposites

In order to study the effects of reaction time on the crystal structure of the synthesized nanocomposites, S2, S3 and S4 are synthesized at 275 °C with 0.5 h, 1.5 h, and 3 h, respectively, as the ratio of iron(III) 2,4-pentanedionate:zinc(II) acetylacetonate: biochar = 4:1:2. S2, S3 and S4 are characterized by XRD and the patterns are shown in Fig. 1a. The diffraction peaks at 30.2°, 35.6°, 43.3°, 57.2°, 62.9° and 74.5° are assigned to γ-Fe_2O_3 magnetite (PDF 39-1346) crystal planes of (2 2 0), (3 1 1), (4 0 0), (5 1 1), (4 4 0) and (5 3 3) respectively, which is consistent with the study of Guivar et al. [25]. It can be observed that the peaks show higher intensities and narrower profile as the reaction time increases from 0.5 h to 3 h, which indicates that the nanoparticles can

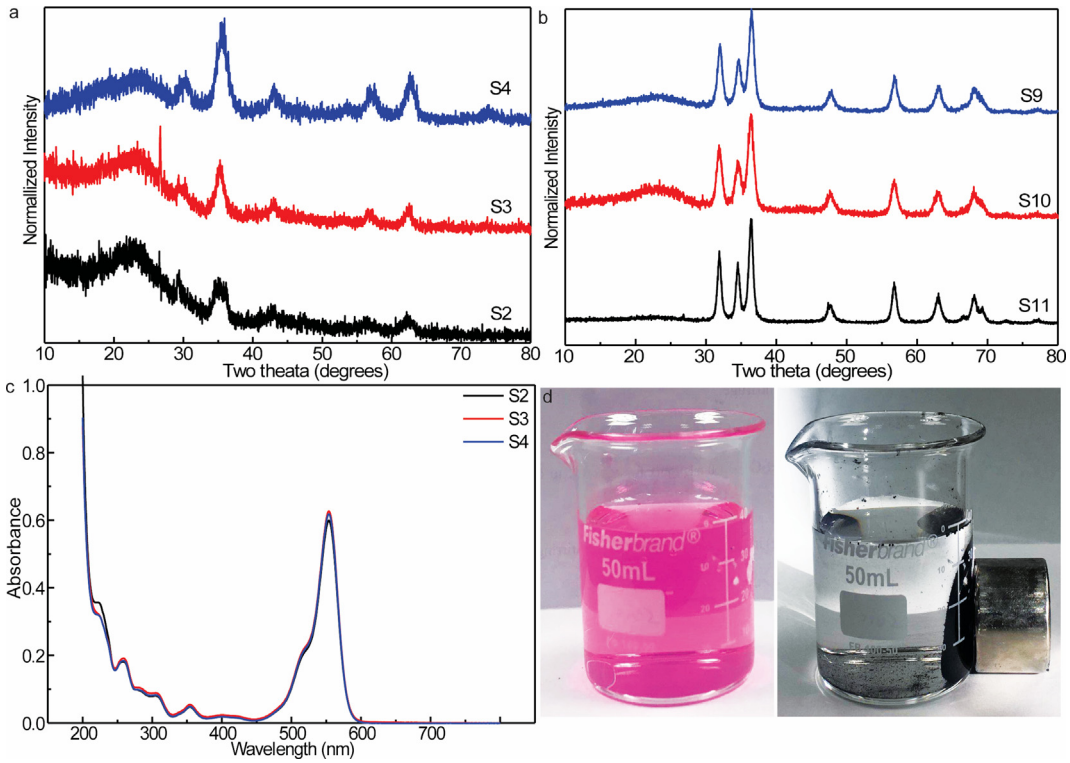

Fig. 1. a XRD patterns of sample S2, S3 and S4, b XRD patterns of sample 9, 10 and 11, c absorption curves of sample S2, S3 and S4 and d the photographs of the dye aqueous solution and the dye solution treated by magnetic nanocomposites.

be formed in the biochar matrix through 0.5 h reaction time and crystallization is improved with the increasing of reaction time. There are no diffraction peaks from ZnO can be observed, which is ascribed to the limited amount of zinc(II) acetylacetonate used in the reaction. ZnO-biochar nanocomposites with different ratios are studied by XRD, and the data are shown in Fig. 1b. The ratios of zinc(II) acetylacetonate: biochar for S9, S10 and S11 are 8:2, 4:2 and 2:2 respectively. Fig. 1b shows that all the nanocomposites are well crystalized. The peaks at 31.8°, 34.5°, 36.3°, 47.7°, 56.7°, 68.1° and 69.3° are indexed to the crystal planes of (1 0 0), (0 0 2), (1 0 1), (1 0 2), (1 1 0), (1 1 2) and (2 0 1) of ZnO (PDF 75-0576). RhB aqueous solutions with the same concentration are treated by S2, S3 and S4 respectively to study the adsorption capabilities of three samples. Fig. 1c shows the UV–vis absorption spectra of RhB aqueous solutions treated by S2, S3 and S4 with the same experimental conditions. The absorbance value (Abs) are 0.599, 0.626 and 0.617 respectively as S2, S3 and S4 are used to treat the RhB aqueous solutions, respectively, indicating that synthesis reaction time has no significant effects on adsorption ability of synthesized biochar nanocomposites. Therefore, in this study, 0.5 h should be good enough for this synthesis method. Fig. 1d. shows the photographs of the dye aqueous solution and the dye solution treated by γ-Fe_2O_3-ZnO-biochar nanocomposites. The pink color is caused by the RhB. We use our magnetic γ-Fe_2O_3-ZnO-biochar nanocomposites to remove the dye in the solution. A clear solution is obtained in the beaker by adding γ-Fe_2O_3-ZnO-biochar nanocomposites into the beaker, which indicates successful removal of RhB by our magnetic biochar nanocomposites. Then a magnet is placed outside the beaker to drive the magnetic biochar toward the magnet, which confirms the magnetic behavior of our nanocomposite.

The morphology magnetic biochar nanocomposites are studied. Fig. 2a, b and c show the TEM images of S2, S3, and S4, respectively. It can be observed that nanoparticles are loaded on the biochar, and there was no significant difference of the three samples, indicating the reaction time does not affect the composite structure that much. The diameters of the nanoparticles are ~6 nm. TEM images of S9, S10 and S11 are presented in Fig. 2d, e and f respectively. S9, S10 and S11 are ZnO-biochar nanocomposites according to the information of Table 1. Therefore, the nanoparticles in Fig. 2d, e and f are assigned to ZnO nanoparticles, and the diameters of the ZnO nanoparticles in S9, S10 and S11 can be estimated to be about ~20 nm. Based on the TEM images of ZnO- biochar and γ-Fe_2O_3-ZnO-biochar, the nanoparticles with the sizes of ~6 nm in Fig. 2a, b and c are γ-Fe_2O_3 nanoparticles. The HRTEM images are shown in Fig. S1. There are very limited ZnO nanoparticles in S2, S3 and S4, which can be attributed to very limited amount of zinc(II) acetylacetonate starting materials used in the reaction.

The distribution of γ-Fe_2O_3 and ZnO nanoparticles on biochar of S2 is investigated by EDX element mapping images. Fig. 3a, b, c and d show the SEM, C, Fe and Zn element mapping images, respectively. Red color represents C element, green color represents Fe element, and light blue represents Zn element. Fig. 3e, f, g and h show SEM and EDX element mapping images of one small area of S2. It can be seen that the C, Fe and Zn elements distribute uniformly in the biochar matrix, which confirmes homogeneous structure of our nanocomposites. Fig. 3i, j, and k show the SEM and C and Zn element mapping images of S9. Fig. 3l, m, and n show the SEM and C and Zn element mapping images of S10. Fig. 3o, p, and q show the SEM and C and Zn element mapping images of S11. The light blue color representing Zn element is brighten gradually in Fig. 3k, n, and q, indicating Zn element increases in the composite from S9 to S11. This is attributed to the increased ratios of zinc(II) acetylacetonate to biochar used in the reaction according Table 1 from S9 to S11. From the SEM cross section images, it can be seen that the distribution of the elements C, Zn and Fe are very uniform, indicating that the structure of the nanocomposites is very uniform. Therefore, the method we develop to synthesize magnetic biochar nanocomposites here is very promising for the applications of magnetic biochar.

The XPS spectra of S2 and S11 are shown in Figs. S2 and S3 respectively. As shown in Fig. S2 left, the peaks at 285, 530, 711 and 1021 eV can attribute to C1s, O1s, Fe2p, and Zn2p respectively [26,27].

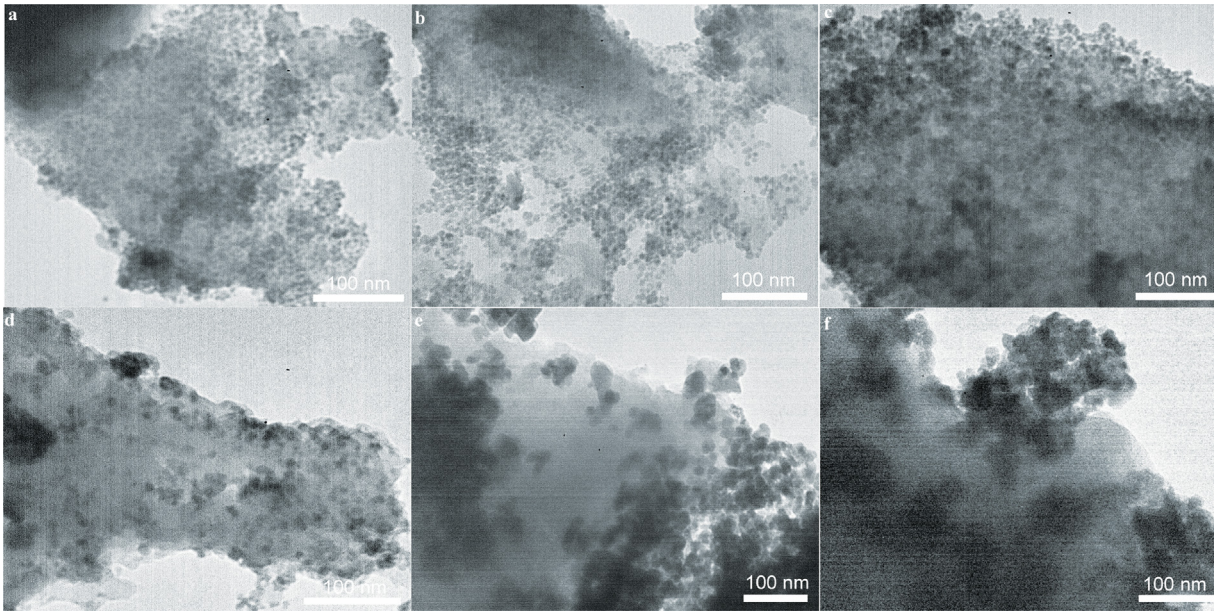

Fig. 2. TEM images of a S2, b S3, c S4, d S9, e S10 and f S11.

As shown in Fig. S2 right, the Fe2p can be mainly fitted to two peaks at 711 eV and 724 eV, which are assigned to $Fe2p_{3/2}$ and $Fe2p_{1/2}$ respectively. A satellite peak at 719 eV indicates the formation of γ-Fe_2O_3 nanoparticlesIn Fig. S3 left, the peaks of O1s and Zn2p are present, confirming the formation of ZnO nanoparticles. As shown in Fig. S3 right, peaks at 1044 eV and 1021 eV are assigned to $Zn2p_{3/2}$ and $Zn2p_{1/2}$ respectively [26]. Tables S1 and S2 show the XPS survey quantification of sample S8 and S11.

N_2-adsorption of pure biochar, sample S8 and S11 are tested, and the results are shown in Fig. S4 and Table S3. Table S3 shows the surface area and pore structure of these samples. The surface area, pore volume and pore size decrease due to γ-Fe_2O_3 and ZnO nanoparticles occupying the active sites of biochar. As shown in Fig. S4, the adsorption isotherm of pure biochar is dominated by monolayer adsorption. However, the adsorption isotherms of S8 and S11 are dominated by the multiple layer adsorption. This difference is attributed to the effect of γ-Fe_2O_3 and ZnO nanoparticles bonded on biochar.

3.2. RhB adsorption using γ-Fe_2O_3-ZnO-biochar nanocomposites

3.2.1. RhB decoloration under UV-light and adsorption using original biochar

It was reported that RhB degrades if it is exposed to UV-light [27,28], in this case, the effects of UV-light on decoloration of RhB need to be investigated prior to adsorption tests. Before irradiation by UV-light, 20 mL 0.01 mol/L of RhB aqueous solution is placed in the dark environment for 15 min (displayed as 0 min in the figures), afterwards, the solution is irradiated under UV-light for another period of time, 10, 20, and 30 min. The UV–vis absorption spectra of RhB solution after UV light irradiation for 10, 20 and 30 min are collected. As shown in Fig. 4a, the original RhB solution has an initial Abs of 0.95. With the irradiation time increased from 10 to 30 min, the Abs values of RhB solutions decreased from 0.93 to 0.88. Therefore, the degradation of RhB caused by UV-light irradiation is not very significant. The results of RhB adsorption using raw biochar is shown in Fig. 4b. It can be seen that after 15 min adsorption in dark environment (0 min), the Abs of RhB solution decreases to 0.51, indicating that residual concentration of RhB in the solution was 1.595 g/L. As a result, the RhB removal percentage is about 66.7% after adsorption for 15 min using bare biochar without UV light irradiation. The Abs of RhB solution are 0.429, 0.377 and 0.365 for the irradiation time of 10, 20 and 30 min, respectively. Consequently, the RhB removal percentage of raw biochar increases to 74.7%, 79.8% and 81.0% after irradiating under UV-light for 10, 20 and 30 min respectively. The increased removal percentages are attributed to the RhB degradation due to UV-light irradiation [29].

3.2.2. Photocatalyst properties of ZnO-biochar nanocomposites

To evaluate the photocatalyst properties of ZnO-biochar nanocomposites, S9, S10 and S11 are used for RhB decoloration test. The RhB solutions with a concentration of 0.01 mol/L are used for the adsorption tests. The decoloration rate is defined as Eq. (2):

$$R = (Abs_{initial} - Abs_{final})/Abs_{initial} \quad (2)$$

The $Abs_{initial}$ in Eq. (1) is 0.95 and Abs_{final} is measured by UV–vis when a test time was reached. From Fig. 5, it can be clearly observed that ZnO-biochar nanocomposites can decolor the RhB solutions greatly. The Abs of RhB solutions treated with S9 are 0.665, 0.396, 0.273 and 0.110 after irradiation under UV-light for 0, 10, 20 and 30 min, respectively (Fig. 5a), leading to that RhB decoloration rate processed by S9 is about 88.63%. In Fig. 5b, it is obvious that the Abs of RhB treated with S10 is lower than that of S9. The Abs of RhB solution is 0.63 without irritation by UV-light, and this number decreased to about 0.02 after irradiation by UV-light for 30 min. In Fig. 5c, the Abs of RhB solution decreased from 0.48 decreases to 0.003 as S11 is used to treat the RhB solution. The decoloration rate of RhB for S11 is up to ~100% after irradiation for 30 min. This is consisted with the published results [30,31]. This could be attributed to the relative ZnO amount in S11 is much larger than the other two samples. Therefore, ZnO can improve the decoloration of RhB due to the improved dye removal capabilities caused by photocatalysis properties.

3.2.3. Effect of ZnO amount in γ-Fe_2O_3-ZnO-biochar on the RhB removal test

In order to evaluate the effects of ZnO amount contained in γ-Fe_2O_3-ZnO-biochar nanocomposites on the adsorption of RhB, tests are performed on S1, S2, S7 and S8. The ratios of iron(III) 2,4-pentanedionate:zinc(II) acetylacetonate: biochar are 4:0:2, 4:1:2, 4:2:2 and 4:4:2 for S1 S2 S7 and S8, respectively. Therefore, ZnO amount increases from S1 to S8 in these four samples. As shown in Fig. 6a, the RhB Abs of S1 is 0.6, 0.56, 0.54 and 0.46 after UV-light irradiation for 0, 10, 20 and 30 min respectively. As a result, the RhB adsorption percentage was 57.8%, 61.7%, 63.8% and 71.9% for 0, 10, 20 and 30 min respectively.

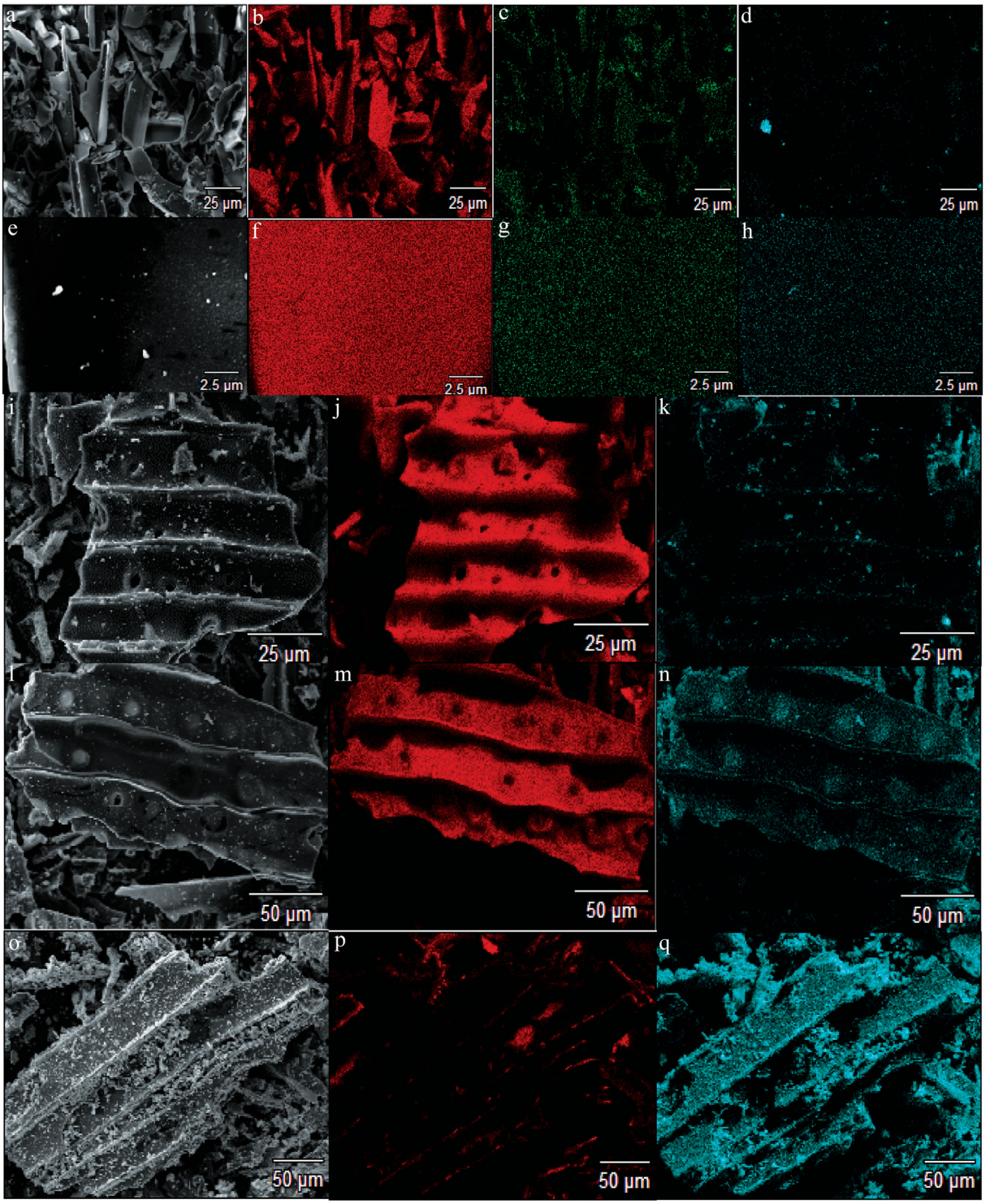

Fig. 3. SEM images and EDX element mapping images. A, b, c, and d for S2. e, f, g, and h for small area of S2. I, j, and k for S9. L, m, and n for S10. o, p, q for S11. In the figure, Red color represents C element, Green color represents Fe and Light blue represents Zn. (For interpretation of the references to color in this figure legend, the reader is referred to the web version of this article.)

Compared with the original biochar (data in Fig. 4b), S1 has a lower removal percentage of RhB. Note that there are no ZnO nanoparticles existed in S1. γ-Fe_2O_3 nanoparticles have negative effects on the adsorption capability of biochar. This phenomenon was also reported in other's publications [32,33]. Some pores of biochar are filled with γ-Fe_2O_3 nanoparticles, leading to decreased activate sites of biochar and reduced adsorption capability. The UV–vis absorption spectra of RhB treated with S2 are illustrated in Fig. 6b. It can be seen that RhB solution shows Abs of 0.625 as RhB solution is treated by S2 without UV-light irradiation. It is worth noting that the Abs values of RhB solutions are 0.528, 0.525 and 0.508 after irradiating for 10, 20 and 30 min respectively. These values are lower than that of biochar under the same conditions (Fig. 4b), which indicates that insufficient amount of ZnO have no promotion on RhB removal. As a result, the RhB removal percentage for S2 is 66.9% obtained by irradiating for 30 min. Fig. 6c shows the UV–vis absorption spectra of RhB solution treated by

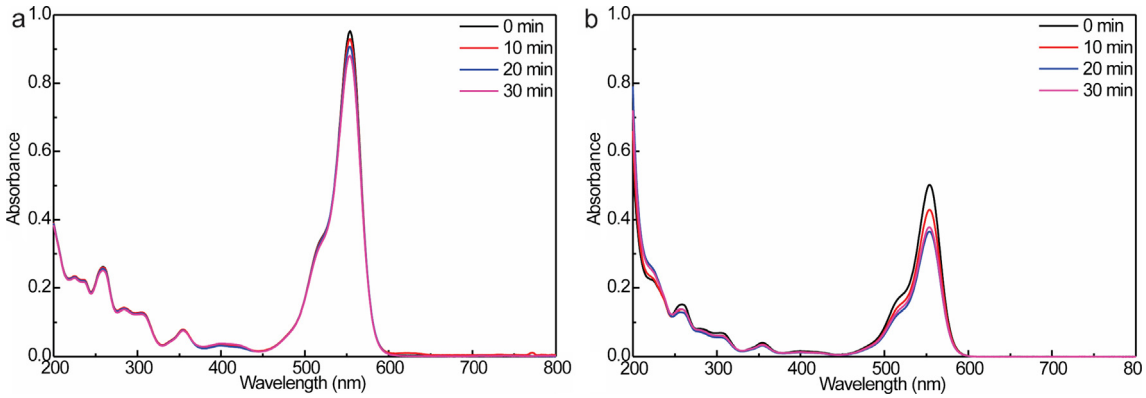

Fig. 4. Plot of a RhB degradation under UV-light (0 min means the original Abs of RhB) and b RhB adsorption using raw biochar (0 min means the RhB solution adsorbed by adsorbents for 15 min without UV-light).

S7. The Abs values of RhB solution decrease dramatically to 0.61, 0.404, 0.373 and 0.276 under irradiation of UV-light for 0, 10, 20 and 30 min UV light irradiation respectively. The corresponding removal percentage values are 56.9%, 77.1%, 80.2% and 89.7%. Liu et al. reported that ZnO nanoparticle have superior photocatalytic activity [31]. Therefore, the decreased Abs of RhB solutions after adsorption by S7 is attributed to photocatalytic properties of ZnO. In S8, ZnO amount further increases (Fig. 6d). The Abs decreases from 0.601 to 0.312 when UV-light irradiation time increases from 0 to 30 min. The RhB removal percentages are 57.7%, 70.3%, 79.4% and 86.2% after UV light irradiation for 0, 10, 20 and 30 min, respectively. Base on RhB removal performance of S1, S2, S7 and S8, it can be found that S7 shows better adsorption performance than other samples. The removal efficiency of pure biochar is compared with our γ-Fe_2O_3-ZnO nanocomposites with 0.5 h UV light irritation, and the absorption spectra after irritation are shown in Fig. S5. As shown in Fig. S5, the absorbance of RhB solution after treated with biochar, S4, S7, S8, S9, S10 and S11 are 0.378, 0.368, 0.276, 0.311, 0.111, 0.017 and 0.003 respectively, indicating higher removal abilities of these γ-Fe_2O_3-ZnO-biochar nanocomposites compared with pure biochar due to the photodecoloration effect of nanoparticles. When the amount of ZnO is lower than a certain value, the negative effect of ZnO is greater than its positive effect since the loaded ZnO nanoparticles occupy the activated site on the biochar, leading to reduced adsorption ability of biochar. The photocatalysis properties dominate the effects of ZnO as more ZnO nanoparticles are introduced to the biochar, leading to increased RhB removal efficiency. As ZnO amount further increases, ZnO nanoparticles block the light, resulting in reduced photocatalysis effect and RhB removal efficiency. This is consistent with the results of Tian et al. [30] in MoS_2/ZnO composite structure.

In order to check the stability of nanocomposites, the TEM and SEM images of our samples before and after photodecoloration experiments were compared. Fig. S6 shows TEM image of sample S8 before and after photodecoloration experiment. No significant structure change of the composites can be observed. Figs. S7 and S8 show EDX element mapping images of sample S8 before and after photodecoloration experiment repectively. It can be seen both Fe and Zn elements are distributed on biochar surface uniformly, indicating the good stability of γ-Fe_2O_3 and ZnO nanoparticles on biochar.

4. Conclusions

In this work, we develop a method to synthesize γ-Fe_2O_3-ZnO-biochar nanocomposites in triethylene glycol using a thermal decomposition method under the protection of N_2 gas. This method avoids high temperature treatment process. The prepared nanocomposites are characterized and their adsorption performance on RhB is investigated. The nanocomposites show very uniform structure, and the ratios of γ-Fe_2O_3:ZnO:biochar are controlled by the ratios of the staring materials to optimize the adsorption performance on RhB removal. The

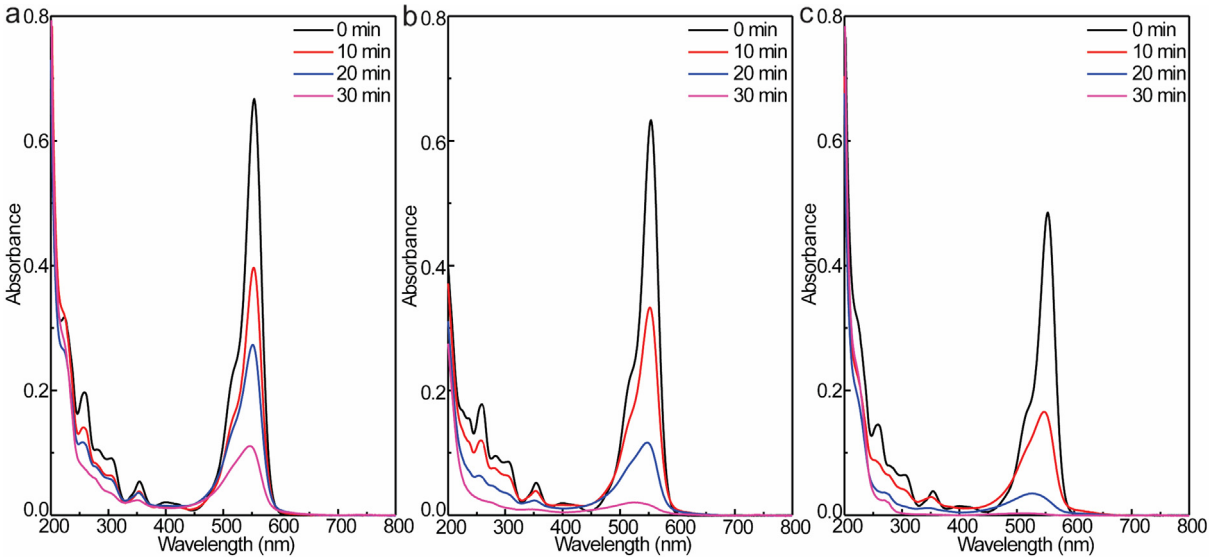

Fig. 5. Photocatalyst properties of ZnO-biochar nanocomposites, a S9, b S10 and c S11.

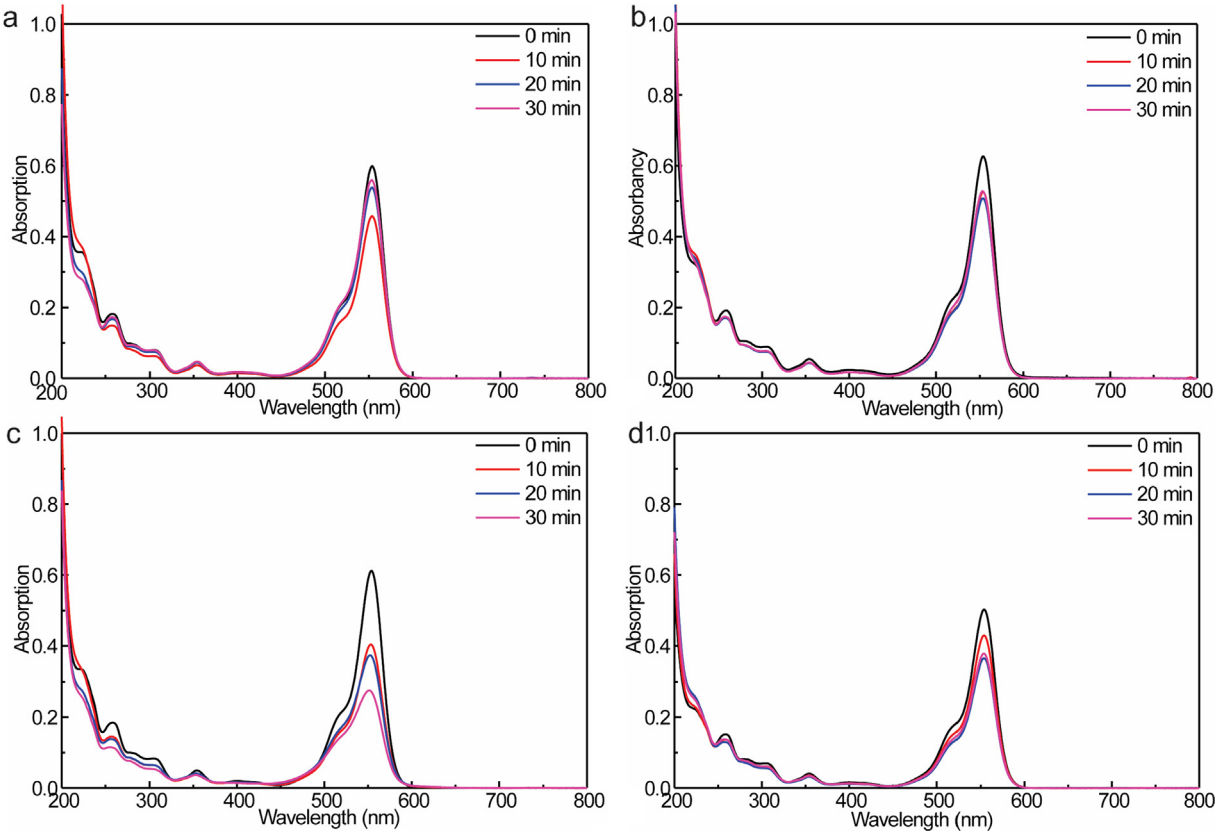

Fig. 6. Effect of ZnO amount on RhB adsorption of a S1, b S2, c S7 and d S8.

synthesized γ-Fe_2O_3-ZnO-biochar nanocomposites can be easily separate from aqueous solution. Photocatalysis properties of ZnO are used to improve the RhB adsorption capability, and the nanocomposites with optimized ratios are obtained toward high RhB adsorption capability.

Acknowledgements

This work was supported by National Science Foundation Award #1632899. DariaWeathersb was supported by Department of Education [Award #P120A170075]. The XRD and TriStar II Plus used in this work was supported by the U.S. Army Engineer Research and Development Center (W912HZ-16-2-0021). The XPS instrument used in this work was supported by a Major Research Instrumentation grant from the National Science Foundation (Award DMR-1726901).

Appendix A. Supplementary material

Supplementary data to this article can be found online at https://doi.org/10.1016/j.apsusc.2019.144217.

References

[1] C.-Z. Liang, S.-P. Sun, B.-W. Zhao, T.-S. Chung, Ind. Eng. Chem. Res. 54 (2015) 11159–11166.
[2] T. Rasheed, M. Bilal, H.M. Iqbal, H. Hu, X. Zhang, Water Air, & Soil Pollut. 228 (2017) 291.
[3] D.M. de Araujo, C. Saez, C.A. Martinez-Huitle, P. Canizares, M.A. Rodrigo, Appl. Catal. B: Environ. 167 (2015) 454–459.
[4] T. Maneerung, J. Liew, Y. Dai, S. Kawi, C. Chong, C.-H. Wang, Bioresour. Technol. 200 (2016) 350–359.
[5] S. Han, K. Liu, L. Hu, F. Teng, P. Yu, Y. Zhu, Sci. Rep. 7 (2017) 43599.
[6] M. Tuzen, A. Sarı, T.A. Saleh, J. Environ. Manage. 206 (2018) 170–177.
[7] B. Kavitha, P.V.L. Reddy, B. Kim, S.S. Lee, S.K. Pandey, K.-H. Kim, J. Environ. Manage. 227 (2018) 146–154.
[8] F.-L. Fan, Z. Qin, J. Bai, W.-D. Rong, F.-Y. Fan, W. Tian, X.-L. Wu, Y. Wang, L. Zhao, J. Environ. Radioact. 106 (2012) 40–46.
[9] P. Devi, A.K. Saroha, Bioresour. Technol. 169 (2014) 525–531.
[10] C. Chang, F. Lian, L. Zhu, Environ. Pollut. 159 (2011) 2507–2514.
[11] D. Das, M. Sureshkumar, S. Koley, N. Mithal, C. Pillai, J. Radioanal. Nucl. Chem. 285 (2010) 447–454.
[12] K. Thines, E. Abdullah, N. Mubarak, M. Ruthiraan, Renew. Sustain. Energy Rev. 67 (2017) 257–276.
[13] Q. Wang, J. Qiao, J. Zhou, S.J.E.A. Gao, Electrochim. Acta 167 (2015) 470–475.
[14] Q. Wang, Z. Liu, R. Jin, Y. Wang, S.J.S. Gao, P. Technol. 210 (2019) 798–803.
[15] Q. Wang, R. Jin, C. Yin, M. Wang, J. Wang, S.J.S. Gao, P. Technol. 172 (2017) 303–309.
[16] A. Marronnier, H. Lee, H. Lee, M. Kim, C. Eypert, J.-P. Gaston, G. Roma, D. Tondelier, B. Geffroy, Y.J.S.E.M. Bonnassieux, S. Cells 178 (2018) 179–185.
[17] Q. Wang, Z. Liu, H. Feng, R. Jin, S. Zhang, S.J.C.I. Gao, Ceram. Int. 45 (2019) 3995–4002.
[18] M. Samadi, M. Zirak, A. Naseri, M. Kheirabadi, M. Ebrahimi, A.Z. Moshfegh, Res. Chem. Intermed. 45 (2019) 2197–2254.
[19] R. Ebrahimi, A. Maleki, Y. Zandsalimi, R. Ghanbari, B. Shahmoradi, R. Rezaee, M. Safari, S.W. Joo, H. Daraei, S.H. Puttaiah, O. Giahi, J. Ind. Eng. Chem. 73 (2019) 297–305.
[20] S. Prabhu, S. Megala, S. Harish, M. Navaneethan, P. Maadeswaran, S. Sohila, R.J.A.S.S. Ramesh, Appl. Surf. Sci. 487 (2019) 1279–1288.
[21] C. Lunkham, P. Ngernchuklin, C. Ponchio, Key Engineering Materials, Trans Tech Publ., 2019, pp. 404–411.
[22] W. Zhao, H. Li, Z. Liu, D. Wang, S. Liu, Sol. Energy Mater. Sol. Cells 182 (2018) 263–271.
[23] J. Bhattacharya, A. Peera, P.H. Joshi, R. Biswas, V.L. Dalal, Sol. Energ. Mat. Sol. Cells 179 (2018) 95–101.
[24] Z. Zang, X.J.J.o.A. Tang, Compounds 619 (2015) 98–101.
[25] J.A.R. Guivar1, A.I. Martínez, A.O. Anaya, L.D.L.S. Valladares, L.L. Félix, A.B. Dominguez, Adv. Nanopart. 3 (2014) 114–121.
[26] R. Al-Gaashani, S. Radiman, A. Daud, N. Tabet, Y.J.C.I. Al-Douri, Ceram. Int. 39 (2013) 2283–2292.
[27] N. Daneshvar, M. Behnajady, M.K.A. Mohammadi, M.S. Dorraji, Desalination 230 (2008) 16–26.
[28] A. Giwa, P.O. Nkeonye, K.A. Bello, K.A. Kolawole, J. Environ. Protect. 3 (2012) 1063.
[29] Z. Xiong, L.L. Zhang, J. Ma, X. Zhao, Chem. Commun. 46 (2010) 6099–6101.
[30] Q. Tian, W. Wu, S. Yang, J. Liu, W. Yao, F. Ren, C. Jiang, Nanoscale Res. Lett. 12 (2017) 221.
[31] Z. Liu, F.-S. Zhang, Desalination 267 (2011) 101–106.
[32] K.-W. Jung, B.H. Choi, T.-U. Jeong, K.-H. Ahn, Bioresour. Technol. 220 (2016) 672–676.
[33] A. Kumar, G. Sharma, M. Naushad, A. Kumar, S. Kalia, C. Guo, G.T. Mola, J. Photochem. Photobiol., A 337 (2017) 118–131.